Semiconductor Science and Technology

PAPER • OPEN ACCESS

Proton irradiation influence on gate-channel low-field carrier mobility of AlGaN/GaN HEMTs

To cite this article: Qizheng Ji *et al* 2023 *Semicond. Sci. Technol.* **38** 085010

View the article online for updates and enhancements.

You may also like

- Proton-induced single-event effect and influence of annealing on multiple feature size NAND flash memory
Cong Peng, Wei Chen, Yinhong Luo et al.
- Enhancement of radiation hardness of InP-based HEMT with double Si-doped plane
Ying-Hui Zhong, , Bo Yang et al.
- An insight to current collapse in GaN HEMT and suppressing techniques
Pichingla Kharei, Achinta Baidya, Niladri Pratap Maity et al.

This content was downloaded from IP address 107.175.119.148 on 01/10/2023 at 20:40

OPEN ACCESS
IOP Publishing

Semiconductor Science and Technology

Semicond. Sci. Technol. **38** (2023) 085010 (9pp)

https://doi.org/10.1088/1361-6641/ace1a1

Proton irradiation influence on gate-channel low-field carrier mobility of AlGaN/GaN HEMTs

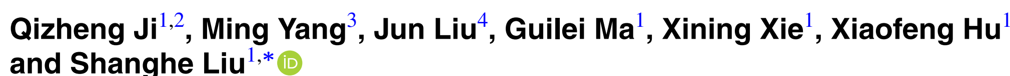

Qizheng Ji[1,2], Ming Yang[3], Jun Liu[4], Guilei Ma[1], Xining Xie[1], Xiaofeng Hu[1] and Shanghe Liu[1,*]

[1] Army Engineering University, Shijiazhuang Campus, National Key Laboratory on Electromagnetic Environment Effects, Shijiazhuang 050003, People's Republic of China

[2] Beijing Institute of Spacecraft Environment Engineering, Beijing 100094, People's Republic of China

[3] Beijing Orient Institute of Measurement and Test, Beijing 100094, People's Republic of China

[4] School of Electronics & Information Engineering, Nanjing University of Information Science & Technology, Nanjing 210044, People's Republic of China

E-mail: liu_sh_h@163.com

Received 29 January 2023, revised 28 April 2023
Accepted for publication 26 June 2023
Published 10 July 2023

Abstract

AlGaN/GaN high electron mobility transistors (HEMTs) with different device sizes were prepared and exposed to 0.4 MeV proton irradiation. The low-field carrier transport characteristics of the gate channel are obtained from the capacitance-voltage curves and current-voltage curves. For the device with a longer gate-drain distance (30 µm), after 0.4 MeV proton irradiation, the gate-channel low-field carrier mobility increases by 14.3% on average. For the device with a shorter gate-drain distance (15 µm), the carrier mobility decreases by 13.4% on average after proton irradiation. This phenomenon is studied with regard to the polarization scattering effect. It is found that the polarization distribution in the AlGaN/GaN HEMTs changes after proton irradiation and different gate-drain distances correspond to different polarization distributions.

Keywords: AlGaN/GaN HEMT, proton irradiation, polarization, scattering

(Some figures may appear in colour only in the online journal)

1. Introduction

The AlGaN/GaN high electron mobility transistor (HEMT) possesses a lot of advantages, such as a high breakdown voltage, high carrier mobility and high carrier saturation velocity [1–3]. Excellent performance makes the AlGaN/GaN HEMT especially suitable for applications in aerospace technology [1–6]. Since outer space is filled with protons, the proton irradiation effect is a main focus in aerospace applications. Although the excellent irradiation resistance of GaN has been proven in theory, the growth process of epitaxial layers is accompanied by lattice mismatch and thermal mismatch between epitaxial layers, which make for a high density of defects. Moreover, the device preparation process, such as thermal annealing, will induce serious lattice damage [7, 8]. This makes the irradiation resistance of AlGaN/GaN HEMT greatly challenging. Although many studies have focussed on the proton irradiation effect of the AlGaN/GaN HEMT, the micro-mechanism is still not thoroughly clarified [9–14].

* Author to whom any correspondence should be addressed.

Original content from this work may be used under the terms of the Creative Commons Attribution 4.0 licence. Any further distribution of this work must maintain attribution to the author(s) and the title of the work, journal citation and DOI.

© 2023 The Author(s). Published by IOP Publishing Ltd

Therefore, the radiation resistance of the AlGaN/GaN HEMT needs to be studied and clarified more systematically in order to take more reliable reinforcement measures.

Proton irradiation may induce displacement damage. Previous studies mainly focus on the defects, which are induced by displacement damage and are able to capture and scatter carriers [9–14]. This explanation is effective for Si-based semiconductors as well GaN-based semiconductors. However, what is different for AlGaN/GaN HEMTs, is that the displacement damage will inevitably change the strain distribution at the AlGaN/GaN interface, which may in turn affect the polarization charge distribution. The polarization charge distribution is closely related to carrier mobility in the view of polarization Coulomb field (PCF) scattering, which has been proven as an important and specific scattering mechanism in AlGaN/GaN HEMTs [15–19]. PCF scattering originates from the nonuniform polarization charges at the AlGaN/GaN interface and is directly related to the device size. The proton irradiation affecting the PCF scattering of AlGaN/GaN HEMTs with different sizes has not been considered in previous studies [9–14]. Therefore, a study of the proton influence on the carrier transport characteristics of AlGaN/GaN HEMT with regard to PCF scattering is significant toward the proposal of irradiation reinforcement measures.

In this paper, AlGaN/GaN HEMTs with four different gate-drain distances were prepared, and the capacitance-voltage (C–V) curves and current–voltage (I–V) curves were measured. The main scattering mechanisms are extracted separately, and the proton irradiation influence on the gate-channel low-field carrier transport characteristics is analyzed.

2. Experiment

The AlGaN/GaN HEMTs used in this paper were fabricated based on AlGaN/GaN heterostructure material. The AlGaN/GaN heterostructure material was fabricated by metal-organic chemical vapor deposition on a Si substrate. The epitaxial layers consist of a 3.9 µm GaN buffer layer, 0.26 µm i-GaN layer, 27.5 nm $Al_{0.25}Ga_{0.75}N$ barrier layer, and a 3.3 nm GaN cap layer. The material structure is shown in figure 1.

AlGaN/GaN HEMTs were fabricated by the traditional process. As shown in figure 2, the source and drain are both Ohmic contacts and the gate is a Schottky contact. Ti/Al/Ni/Au as the Ohmic contacts were deposited on the material by e-beam evaporation and lift-off, which then were annealed in an ambient N_2 environment at 800 °C for 30 s in a rapid thermal annealing system. Using Ni/Au, the Schottky contacts were created by e-beam evaporation. The gate length L_G is 4 µm. The gate width W_G is 104 µm. The gate-source distance L_{GS} is 4 µm. The gate-drain distances L_{GD} are 30 µm, 25 µm, 20 µm and 15 µm, which are marked as Device 1, Device 2, Device 3 and Device 4, respectively. The proton irradiation experiment was performed at the GIC4117 accelerator with 0.4 MeV protons at a fluence of 2.16 × 10^{12} cm^{-2} (beam current 7 pA) and at room temperature. Protons irradiated the upper surface of the devices directly. During the whole irradiation process, the temperature was measured and the maximum temperature rise was only 0.6 K. The C–V curves (at 1 MHz) and I–V curves of the devices were measured at room temperature using a Keithley 4200 A semiconductor parameter analyzer, before and after proton irradiation. The Hall mobility of the AlGaN/GaN heterostructure material was measured at 300 K and 77 K from the Hall measurements before and after proton irradiation, and is shown in table 1. The Hall mobility both decreased at 300 K and 77 K after 0.4 MeV proton irradiation.

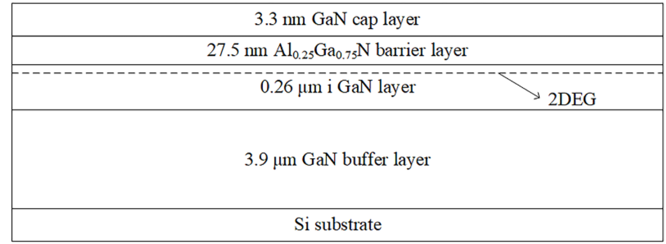

Figure 1. AlGaN/GaN heterostructure material structure.

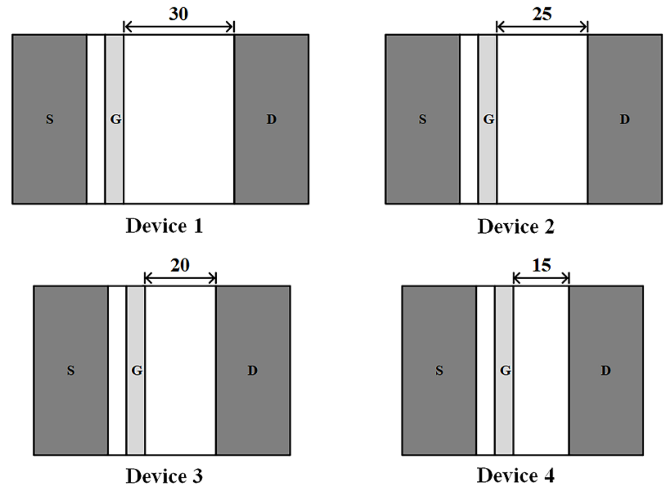

Figure 2. Device structure of AlGaN/GaN HEMTs, unit: µm.

Table 1. Hall mobility at 300 K and 77 K before and after 0.4 MeV proton irradiation.

Temperature	Hall mobility before irradiation (cm^2 V^{-1}·s^{-1})	Hall mobility after irradiation (cm^2 V^{-1}·s^{-1})
300 K	1580	1491
77 K	9225	8972

3. Results and discussion

Figure 3 shows the C–V curves of the fabricated devices before and after proton irradiation. Based on these curves, the electron density (n_{2D}) of the two-dimensional electron gas (2DEG)

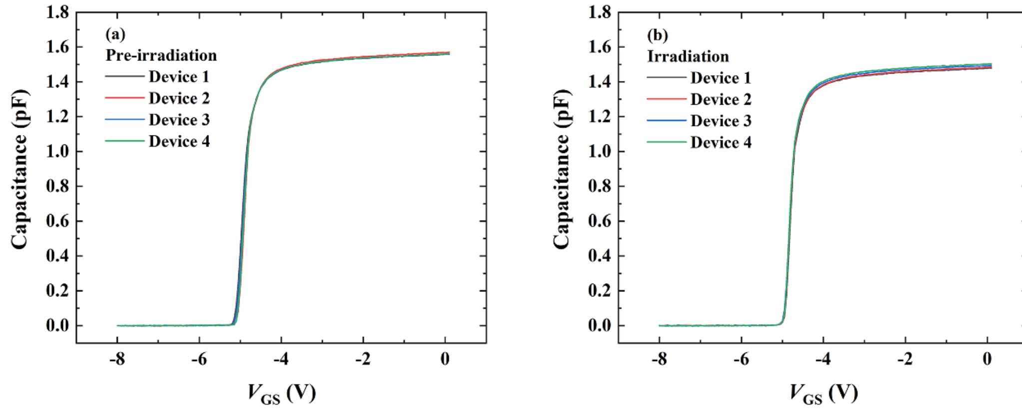

Figure 3. Measured C–V curves before (a) and after (b) proton irradiation for the fabricated AlGaN/GaN HEMTs with different gate-drain distances.

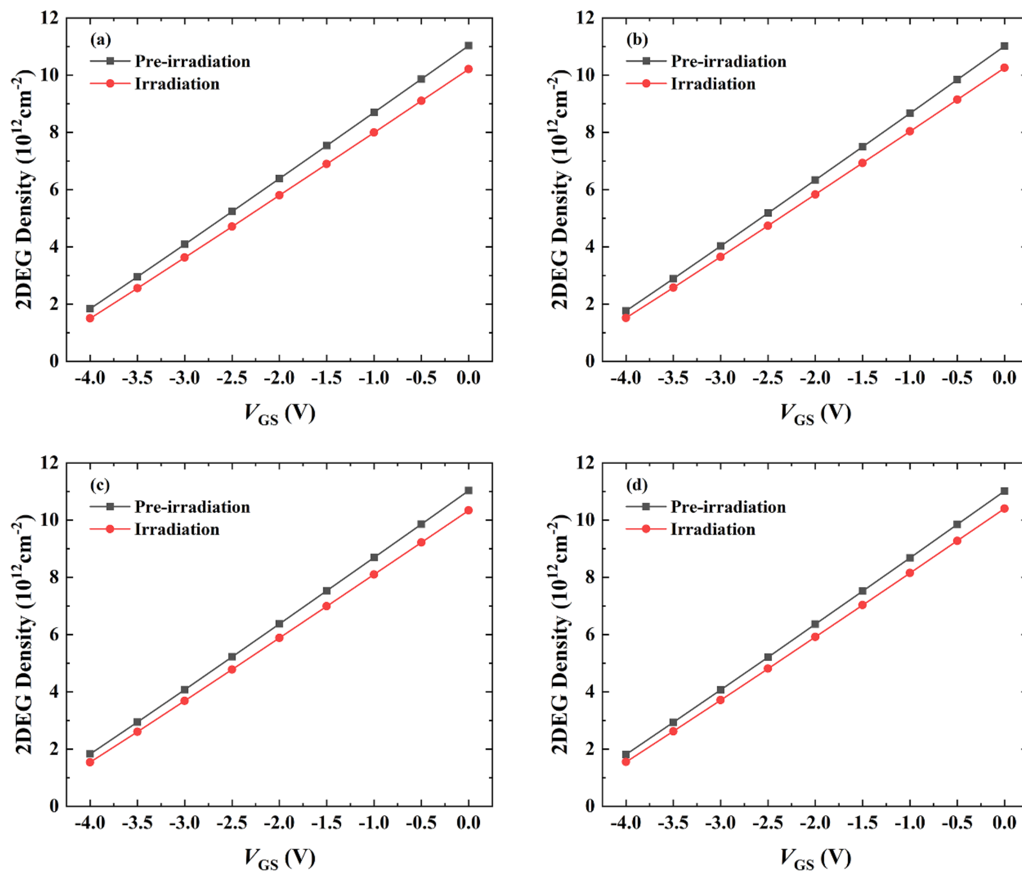

Figure 4. Gate-channel 2DEG electron density n_{2D} as a function of gate voltage for Device 1 (a), Device 2 (b), Device 3 (c) and Device 4 (d).

in the gate channel at different gate voltages can be obtained by following [20]:

$$n_{2D} = \int_{V_T}^{V_{GS}} CdV/(Me), \quad (1)$$

where C is the measured capacitance value, V_T is the threshold voltage, which can be obtained by differentiating the C–V curve, V_{GS} is the gate-source voltage, M is the gate Schottky contact area, and e is the electron charge. The obtained n_{2D} before and after proton irradiation is shown in figure 4. Compared to n_{2D} before proton irradiation, n_{2D} is lower after proton irradiation.

Figure 5 shows the I–V curves before and after proton irradiation of Devices 1–4. As L_{GD} decreases, the drain-source current I_{DS} after irradiation tends to first increase and then decrease compared to before irradiation. According to the

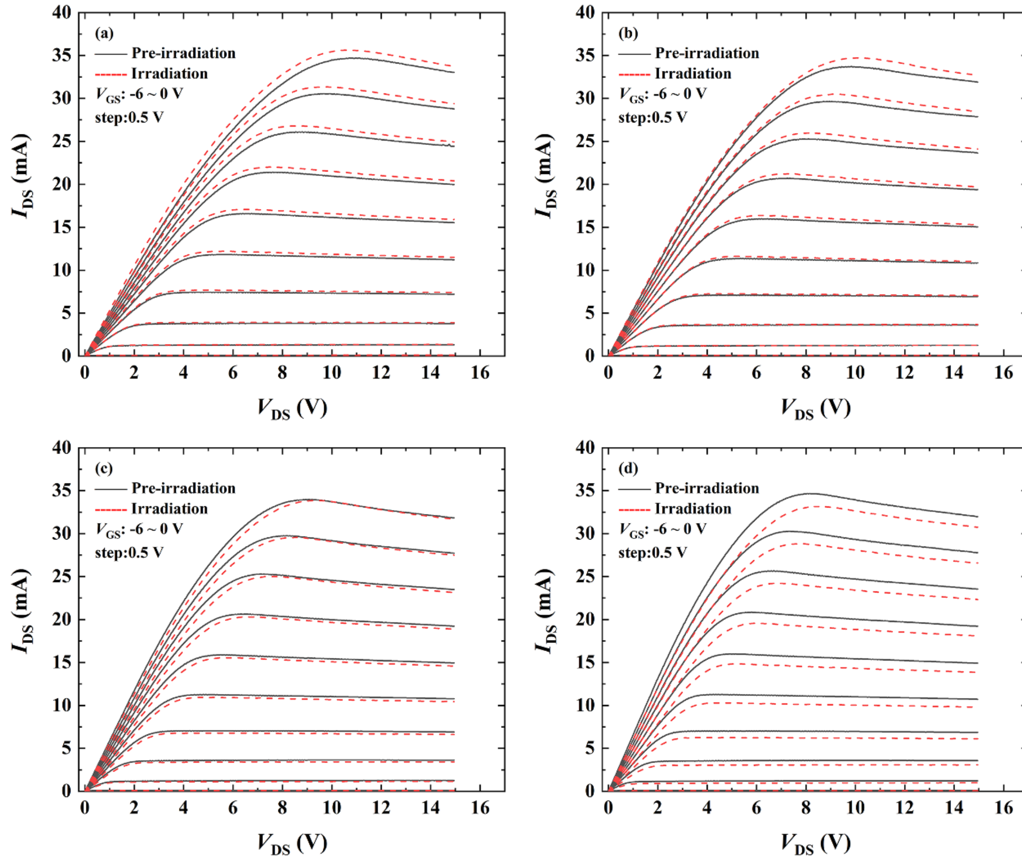

Figure 5. Measured *I–V* curves for Device 1 (a), Device 2 (b), Device 3 (c) and Device 4 (d).

I–V curves and the *C–V* curves, the gate-channel 2DEG electron mobility (μ_n) can be calculated by the following equations [20, 21]:

$$\mu_n = \frac{I_{DS}L_G}{en_{2D}W_G[V_{DS} - I_{DS}(R_d + R_s + 2R_c)]}, \tag{2}$$

$$R_d = \frac{L_{GD}}{en_{2D0}\mu_{n0}W_G}, \tag{3}$$

$$R_s = \frac{L_{GS}}{en_{2D0}\mu_{n0}W_G}, \tag{4}$$

where R_d is the gate-drain access resistance, R_s is the gate-source access resistance, $R_c = 3.54\ \Omega\cdot$mm is the Ohmic contact resistance, which is obtained by the transmission line method. n_{2D0} and μ_{n0} are the 2DEG electron density and electron mobility of the gate channel at $V_{GS} = 0$ V. In this study, the drain-source voltage $V_{DS} = 0.1$ V is chosen because the electron density in the channel at low drain-source fields can be approximated as not varying with the channel position [21–23]. Moreover, according to a previous study [24], the gradient of the polarization charge density at high field is larger than that at low field, inducing the effect where PCF scattering becomes more significant with V_{DS} increasing. Thus, the analysis of low-field mobility offers guidelines for high-field situations.

The obtained gate-channel 2DEG electron mobility is shown in figure 6. The mobility curves of the four devices before irradiation are almost the same. However, the mobility curves after irradiation are obviously separated and decrease as L_{GD} decreases. For Device 1, the 2DEG electron mobility is increased by 14.3% on average after irradiation. For Device 4, the 2DEG electron mobility decreases by 13.4% on average after irradiation. This phenomenon is analyzed as follows.

Mobility is determined by the scattering mechanisms. According to previous studies, the main scattering mechanisms in AlGaN/GaN HEMT are polar optical phonon (POP) scattering, acoustic phonon (AP) scattering, interface roughness (IFR) scattering, dislocation (DIS) scattering and PCF scattering [23, 25, 26]. POP scattering, AP scattering, IFR scattering and DIS scattering are all determined by the inherent properties of the AlGaN/GaN heterostructure material and are not related to device size. Under the influence of these scattering mechanisms, the mobility variation of all four devices should be consistent after irradiation, which is obviously inconsistent with the result in figure 6. PCF scattering has been proven to be closely related to device size. Therefore, the behavior of the electron mobility (figure 6) has to be attributed to PCF scattering.

In order to provide a clearer quantitative analysis, the mobility corresponding to different scattering mechanisms

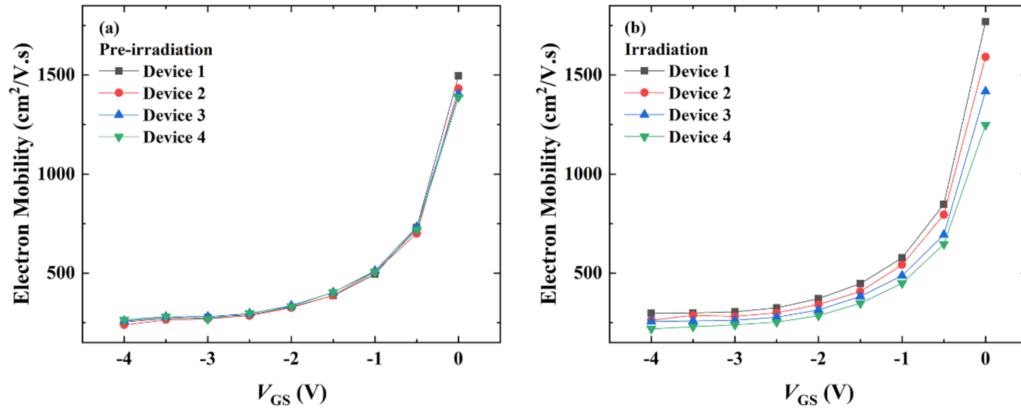

Figure 6. Gate-channel low-field electron mobility before (a) and after (b) proton irradiation as a function of gate voltage for the fabricated AlGaN/GaN HEMTs.

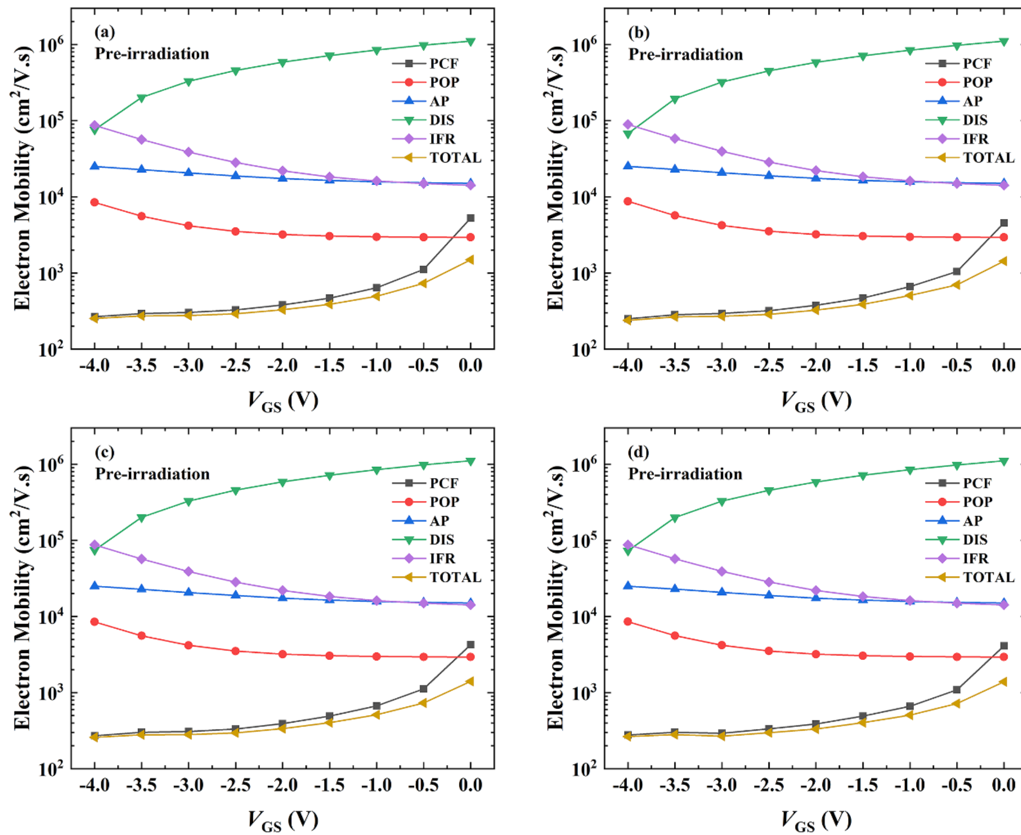

Figure 7. Electron mobility corresponding to PCF, POP, AP, DIS and IFR scatterings, and the experimentally obtained electron mobility (TOTAL) before proton irradiation for Device 1 (a), Device 2 (b), Device 3 (c) and Device 4 (d).

was calculated following the previous studies [22, 26]. Figures 7 and 8 show that the electron mobility before and after proton irradiation corresponds to all the scatterings (μ_{PCF}, μ_{POP}, μ_{AP}, μ_{DIS} and μ_{IFR}) and the total electron mobility (μ_{TOTAL}).

Figure 9 compares the μ_{PCF} of the fabricated four AlGaN/GaN HEMTs before and after proton irradiation. Being similar to figure 6, it is found from figure 9 that the μ_{PCF} curves of the four devices largely overlap before proton irradiation. After irradiation, the μ_{PCF} curves are separated obviously and decrease as L_{GD} decreases.

For a clear comparison, the μ_{PCF} before and after proton irradiation of each device is shown by figure 10. For Device 1, μ_{PCF} gets larger after irradiation. For Device 4, μ_{PCF} gets smaller after irradiation.

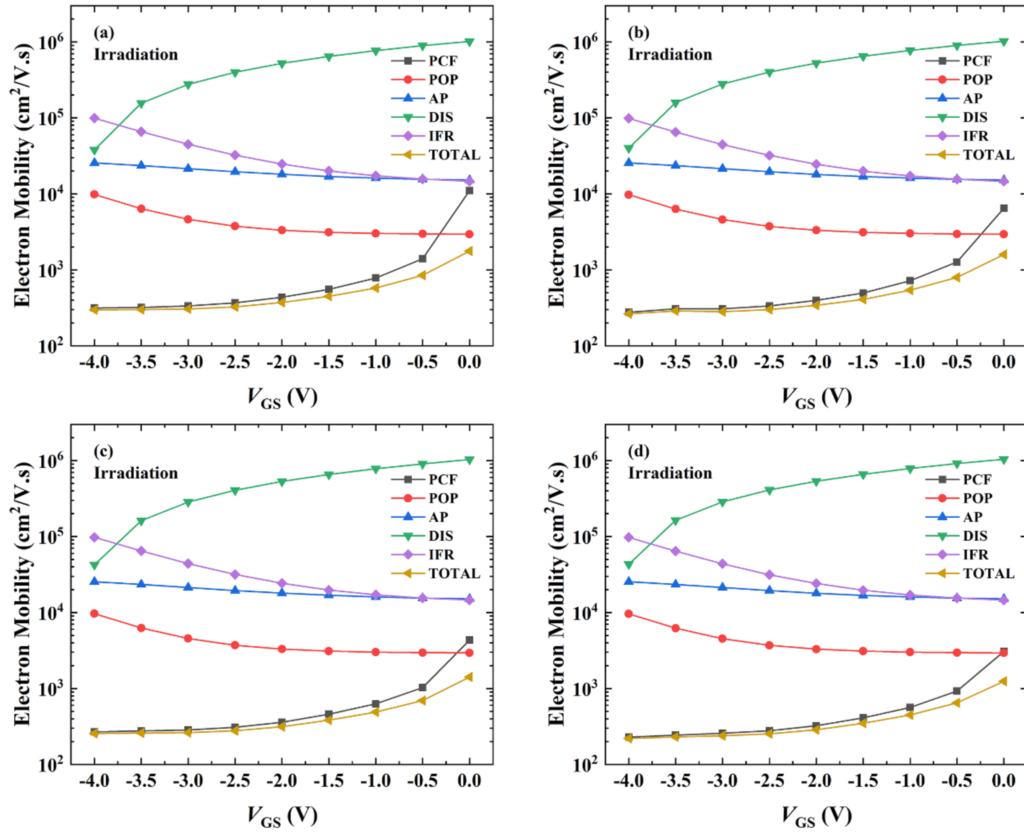

Figure 8. Electron mobility corresponding to PCF, POP, AP, DIS and IFR scatterings, and the experimentally obtained electron mobility (TOTAL) after proton irradiation for Device 1 (a), Device 2 (b), Device 3 (c) and Device 4 (d).

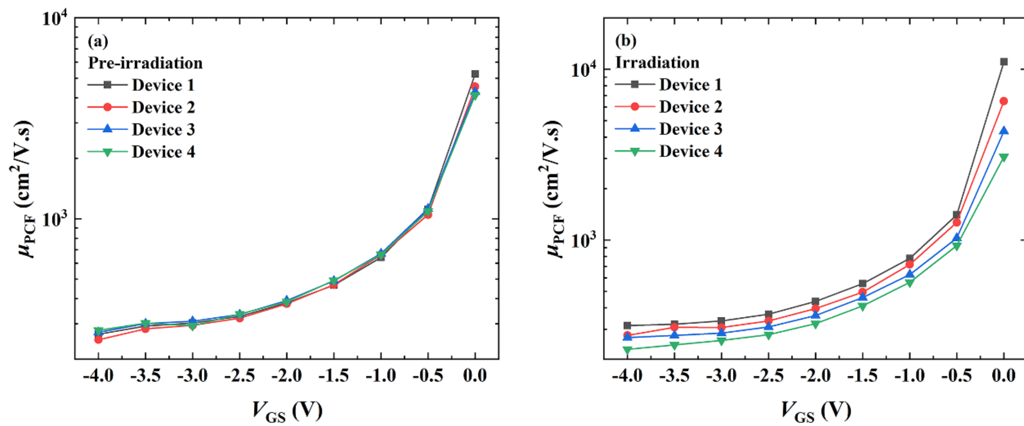

Figure 9. Electron mobility corresponding to PCF scattering μ_{PCF} before (a) and after (b) proton irradiation for the fabricated AlGaN/GaN HEMTs with different gate-drain distances.

Based on the results above, it is quantitatively demonstrated that the different mobility behaviors result from PCF scattering. PCF scattering originates from the nonuniform distribution of polarization charges at the AlGaN/GaN interface. The difference between the nonuniform polarization charges and the original (heterostructure material before device fabrication) uniform polarization charges is called the additional polarization charges $\Delta\sigma$. In this study, the additional polarization charge influence near the Ohmic contact is negligible, which is proved by figure 9(a) [23]. The additional polarization charges at the AlGaN/GaN interface consist of two parts, as shown in figure 11. The applied gate bias changes the strain via the converse piezoelectric effect, generating additional polarization charges $\Delta\sigma_1$ in region I. Since the lattices are interconnected, and the stress (induced by gate bias) in the region I will apply an opposite stress in region II through

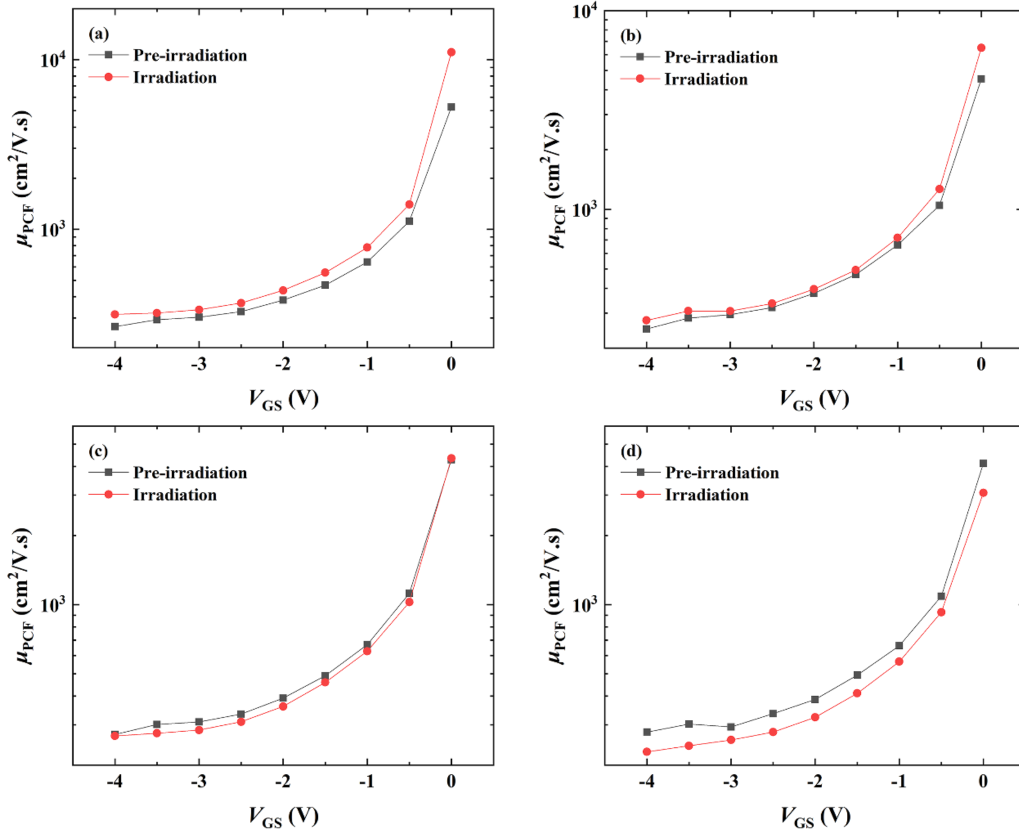

Figure 10. Electron mobility corresponding to PCF scattering μ_{PCF} for Device 1 (a), Device 2 (b), Device 3 (c) and Device 4 (d).

the interconnected lattice, generating $\Delta\sigma_2$ [1, 22]. In addition, the additional polarization charge distribution in region II is expected to be linear, since the degree of lattice variation decreases with increasing distance. The PCF scattering potential $V(x,y,z)$ generated by the additional polarization charges is expressed as follows [23]:

$$V(x,y,z) = -\frac{e}{4\pi\varepsilon_s}\int_{-L_{GS}-\frac{L_G}{2}}^{-\frac{L_G}{2}} dx' \int_0^{W_G} \frac{\Delta\sigma_2\cdot(-x'-L_{GS}-L_G/2)}{L_{GS}\cdot\sqrt{(x-x')^2+(y-y')^2+z^2}} dy' - \frac{e}{4\pi\varepsilon_s}\int_{-\frac{L_G}{2}}^{\frac{L_G}{2}} dx' \int_0^{W_G} \frac{\Delta\sigma_1}{\sqrt{(x-x')^2+(y-y')^2+z^2}} dy' - \frac{e}{4\pi\varepsilon_s}\int_{\frac{L_G}{2}}^{L_{GD}+\frac{L_G}{2}} dx' \int_0^{W_G} \frac{\Delta\sigma_2\cdot(x'-L_{GD}-L_G/2)}{L_{GD}\cdot\sqrt{(x-x')^2+(y-y')^2+z^2}} dy' \quad (5)$$

where ε_s is the GaN dielectric constant. It is obvious that PCF scattering is closely related to the device size and additional polarization charges.

According to figure 9(a) and equation (5), before irradiation, the influence of $\Delta\sigma_2$ is negligible, and $V(x,y,z)$ is dominated by $\Delta\sigma_1$. During proton irradiation, region II lacks the coverage of the gate metal. The protons entering region II enhance the tensile strain of the barrier layer and $\Delta\sigma_2$ turns into $\Delta\sigma_2 + \Delta\sigma_2'$. Since the protons uniformly irradiate the top of the devices, $\Delta\sigma_2'$ is consistent in each device. Due to the lattice continuity, the enhanced tensile strain in region II induces compressive strain or weakens the original tensile strain in region I, with $\Delta\sigma_1$ turning into $\Delta\sigma_1 + \Delta\sigma_1'$. According to equation (5), there is an offsetting effect between positive $\Delta\sigma_2 + \Delta\sigma_2'$ and negative $\Delta\sigma_1 + \Delta\sigma_1'$. A larger L_{GD} will correspond to a stronger offsetting effect. For Device 1, L_{GD} is larger, and the influence of $\Delta\sigma_2 + \Delta\sigma_2'$ is stronger. Following equation (5), the PCF scattering potential gets smaller, and μ_{PCF} becomes larger after irradiation. For Device 4, L_{GD} is smaller, so the integration interval of the last term in equation (5) is smaller and the influence of $\Delta\sigma_2 + \Delta\sigma_2'$ is weaker. As a result, $\Delta\sigma_1 + \Delta\sigma_1'$ plays a dominant role, and the PCF scattering potential gets stronger, inducing a smaller μ_{PCF} after irradiation. This is the reason for the mobility behavior before and after proton irradiation, as shown by figures 6 and 9.

To further verify the above analysis, the n_{2D} variation level Δn_{2D} after proton irradiation at $V_{GS} = 0$ V is compared, as shown by figure 12. Since the 2DEG originates from the strain and polarization charges, the change of n_{2D} can indirectly reflect the strain of the lattice under the gate [1]. It can be found from figure 12 that Δn_{2D} is approximately linear variation as a function of L_{GD}, and Δn_{2D} decreases with L_{GD} increasing. This indicates that, in region I, the compressive strain increases or tensile strain weakens. The larger L_{GD} is, the stronger the effect is. This phenomenon exactly confirms the conclusion of this study.

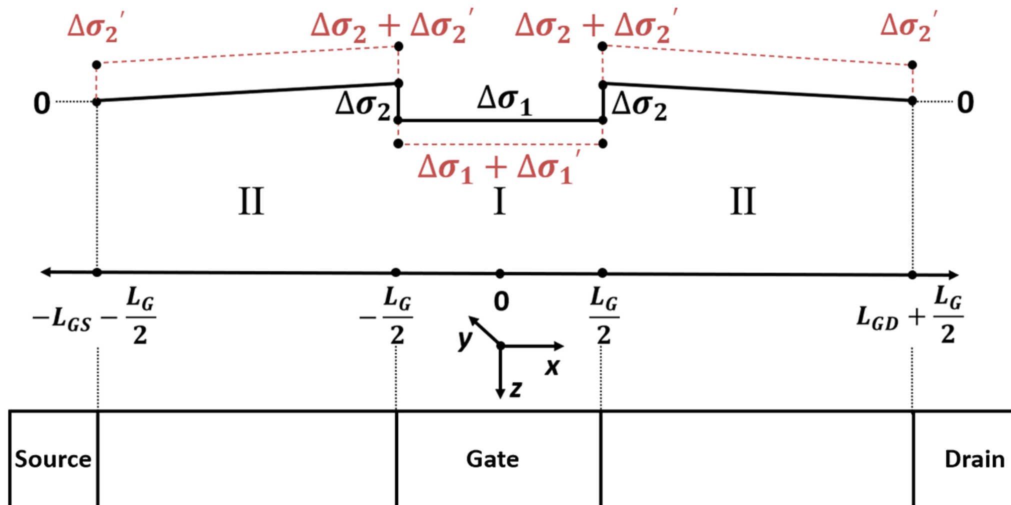

Figure 11. Distribution of polarization charges at the AlGaN/GaN interface.

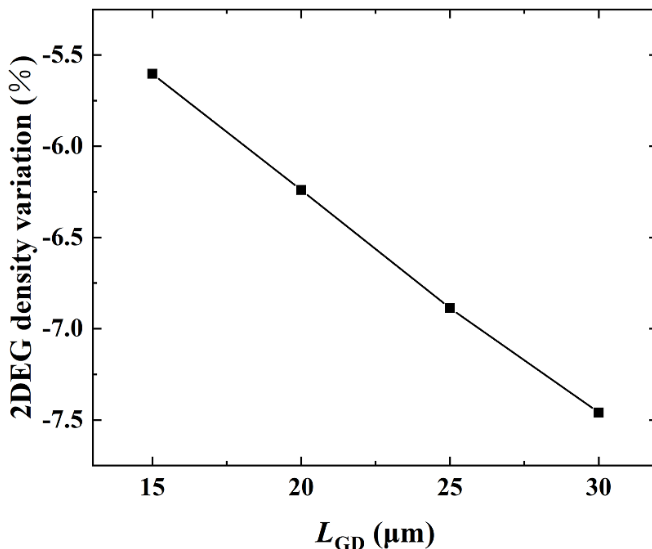

Figure 12. n_{2D} variation level Δn_{2D} after irradiation at gate-source voltage $V_{GS} = 0$ V as a function of gate-drain distance.

4. Conclusion

The proton irradiation influence on gate-channel low-field carrier mobility of AlGaN/GaN HEMTs is analyzed with regard to PCF scattering, which has not been examined in previous studies. It is found that proton irradiation affects the intensity of the PCF scattering by changing the strain and polarization distribution, which in turn influences the carrier mobility of devices. For the device with a 30 μm gate-drain distance, carrier mobility increases due to the decreased intensity of PCF scattering after 0.4 MeV proton irradiation. The carrier mobility of the device with a 15 μm gate-drain distance decreases due to the increasing in PCF scattering intensity after 0.4 MeV proton irradiation. We analyse the variation of PCF scattering with regard to lattice strain, and the lattice strain corresponds to a microcosmic understanding of the influence of proton irradiation on AlGaN/GaN HEMTs. Moreover, the results of the experiment show that the I_{DS} of the device with a larger gate-drain distance gets larger after 0.4 MeV proton irradiation. This means that the performance of AlGaN/GaN HEMTs can be improved by proton irradiation with appropriate energy and fluence. Different gate-drain distances correspond to different trends of current variation after 0.4 MeV proton irradiation, suggesting that adjusting gate-drain distance properly can also provide a new dimension for enhancing the irradiation resistance of devices, which will of benefit for the further optimization of applications in the aerospace field.

Data availability statement

All data that support the findings of this study are included within the article (and any supplementary files).

Acknowledgments

This work was supported by the National Natural Science Foundation of China (Grant No. 61904007).

ORCID iD

Shanghe Liu https://orcid.org/0000-0003-3239-7893

References

[1] Ambacher O *et al* 1999 Two-dimensional electron gases induced by spontaneous and piezoelectric polarization charges in N- and Ga-face AlGaN/GaN heterostructures *J. Appl. Phys.* **85** 3222–33

[2] Khan M A, Kuznia J N, Olson D T, Schaff W J, Burm J W and Shur M S 1994 Microwave performance of a 0.25 μm gate AlGaN/GaN heterostructure field effect transistor *Appl. Phys. Lett.* **65** 1121–3

[3] Wu Y-F, Keller B P, Keller S, Kapolnek D, Denbaars S P and Mishra U K 1996 Measured microwave power performance

of AlGaN/GaN MODFET *IEEE Electron Device Lett.* **17** 455–7
[4] Wu Y-F, Saxler A, Moore M, Smith R P, Sheppard S, Chavarkar P M, Wisleder T, Mishra U K and Parikh P 2004 30-W/mm GaN HEMTs by field plate optimization *IEEE Electron Device Lett.* **25** 117–9
[5] Umana-Membreno G A, Dell J M, Hessler T P, Nener B D, Parish G, Faraone L and Mishra U K 2002 ^{60}Co gamma-irradiation-induced defects in n-GaN *Appl. Phys. Lett.* **80** 4354–6
[6] Khanna S M, Webb J, Tang H, Houdayer A J and Carlone C 2000 2 MeV proton radiation damage studies of gallium nitride films through low temperature photoluminescence spectroscopy measurements *IEEE Trans. Nucl. Sci.* **47** 2322–8
[7] Binari S C, Klein P B and Kazior T E 2002 Trapping effects in GaN and SiC microwave FETs *Proc. IEEE* **90** 1048–58
[8] Divay A, Latry O, Duperrier C and Temcamani F 2016 Ageing of GaN HEMT devices: which degradation indicators? *J. Semicond.* **37** 014001
[9] Hu X, Bo K C, Barnaby H J, Fleetwood D M, Schrimpf R D, Lee S, Shojah-Ardalan S, Wilkins R, Mishra U K and Dettmer R W 2004 The energy dependence of proton-induced degradation in AlGaN/GaN high electron mobility transistors *IEEE Trans. Nucl. Sci.* **51** 293–7
[10] Lv L, Ma J G, Cao Y R, Zhang J C, Zhang W, Li L, Xu S R, Ma X H, Ren X T and Hao Y 2011 Study of proton irradiation effects on AlGaN/GaN high electron mobility transistors *Microelectron. Reliab.* **51** 2168–72
[11] Ives N E, Chen J, Witulski A F, Schrimpf R D, Fleetwood D M, Bruce R W, McCurdy M W, Zhang E X and Massengill L W 2015 Effects of proton-induced displacement damage on gallium nitride HEMTs in RF power amplifier applications *IEEE Trans. Nucl. Sci.* **62** 2417–22
[12] Lv L, Lin Z Z, Guo H X, Pan X Y and Yan X Y 2021 Effects of proton irradiation on enhancement-mode AlGaN/GaN MIS-HEMTs *Mod. Appl. Phys.* **12** 88–94
[13] He H, He C H, Liao W L, Zhang J H, Zang H and Liu W B 2019 Molecular dynamics simulation of proton irradiation damage in GaN *At. Energy Sci. Technol.* **53** 1117–21
[14] Lv L, Zhang J C, Li L, Ma X H, Cao Y R and Hao Y 2012 Effects of 3 MeV proton irradiation on AlGaN/GaN high electron mobility transistors *Acta Phys. Sin.* **61** 057202
[15] Yuan L, Chen H and Chen K J 2011 Normally off AlGaN/GaN metal–2DEG tunnel-junction field-effect transistors *IEEE Electron Device Lett.* **32** 303–5
[16] Cui P, Liu H, Lin W, Lin Z, Cheng A, Yang M, Liu Y, Fu C, Lv Y and Luan C 2017 Influence of different gate biases and gate lengths on parasitic source access resistance in AlGaN/GaN heterostructure FETs *IEEE Trans. Electron Devices* **64** 1038–44
[17] Lv Y, Lin Z, Meng L, Luan C, Cao Z, Yu Y, Feng Z and Wang Z 2012 Influence of the ratio of gate length to drain-to-source distance on the electron mobility in AlGaN/AlN/GaN heterostructure field-effect transistors *Nanoscale Res. Lett.* **7** 434
[18] Liu Y, Lin Z J, Yang M, Luan C B, Wang Y T, Lv Y J and Feng Z H 2016 Effect of polarization Coulomb field scattering on low temperature electron mobility in strained AlGaN/AlN/GaN heterostructure field-effect transistors *Mod. Phys. Lett.* B **30** 1650411
[19] Yang M, Ji Q, Su X, Zhang W, Wang Y, Wang L, Hu X, Yuan Q, Feng P and Liu Y 2020 Study on the electron mobility related with Ohmic contact width in AlGaN/GaN HEMTs *Mod. Phys. Lett.* B **34** 2150008
[20] Zhao J, Lin Z, Corrigan T D, Wang Z, You Z and Wang Z 2007 Electron mobility related to scattering caused by the strain variation of AlGaN barrier layer in strained AlGaN/GaN heterostructures *Appl. Phys. Lett.* **91** 173507
[21] Lv Y, Lin Z, Zhang Y, Meng L, Luan C, Cao Z, Chen H and Wang Z 2011 Polarization Coulomb field scattering in AlGaN/AlN/GaN heterostructure field-effect transistors *Appl. Phys. Lett.* **98** 123512
[22] Yang M, Lv Y, Cui P, Liu Y, Fu C and Lin Z 2018 Determination of the polarization and strain distribution in AlGaN/GaN heterostructure field-effect transistors *J. Phys. Chem. Solids* **123** 223–7
[23] Luan C, Lin Z, Lv Y, Zhao J, Wang Y, Chen H and Wang Z 2014 Theoretical model of the polarization Coulomb field scattering in strained AlGaN/AlN/GaN heterostructure field-effect transistors *J. Appl. Phys.* **116** 044507
[24] Luan C, Lin Z, Lv Y, Feng Z, Zhao J, Zhou Y, Yang Q and Yang M 2014 Influence of polarization coulomb field scattering on the subthreshold swing in depletion-mode AlGaN/AlN/GaN heterostructure field-effect transistors *Physica* E **62** 76–79
[25] Yang M, Lv Y, Feng Z, Lin W, Cui P, Liu Y, Fu C and Lin Z 2016 Study of source access resistance at direct current quiescent points for AlGaN/GaN heterostructure field-effect transistors *J. Appl. Phys.* **119** 224501
[26] Gurusinghe M N, Davidsson S K and Andersson T G 2005 Two-dimensional electron mobility limitation mechanisms in $Al_xGa_{1-x}N$/GaN heterostructures *Phys. Rev.* B **72** 045316